

Transient Stability Assessment of Networked Microgrids Using Neural Lyapunov Methods

Tong Huang, *Student Member, IEEE*, Sicun Gao, and Le Xie, *Senior Member, IEEE*

Abstract—This paper proposes a novel transient stability assessment tool for networked microgrids based on neural Lyapunov methods. Assessing transient stability is formulated as a problem of estimating the dynamic security region of networked microgrids. We leverage neural networks to learn a local Lyapunov function in the state space. The largest security region is estimated based on the learned neural Lyapunov function, and it is used for characterizing disturbances that the networked microgrids can tolerate. The proposed method is tested and validated in a grid-connected microgrid, three networked microgrids with mixed interface dynamics, and the IEEE 123-node feeder. Case studies suggest that the proposed method can address networked microgrids with heterogeneous interface dynamics, and in comparison with conventional methods that are based on quadratic Lyapunov functions, can characterize the security regions with much less conservativeness.

Index Terms—Networked microgrids, transient stability assessment, Neural Lyapunov method, energy management system, machine learning, resilient grid

I. INTRODUCTION

The past decade has witnessed increasing deployment of distributed energy resources (DERs) in the electric distribution grid. DERs play a crucial role of decarbonizing the energy sector and enhancing the resilience of the grid. However, deepening penetration of DERs leads to unprecedented complexity for distribution system operation in monitoring, control, and protection. One promising solution to managing massive integration of DERs is to reconfigure the distribution system as *networked microgrids* shown in Figure 1. A microgrid packages interconnected Distributed Generation Units (DGUs) and loads which are regulated locally by the Microgrid Central Controller (MGCC) [1]. The microgrid has a power-electronic (PE) interface [1], [2] that physically connects to its host distribution system via a point of common coupling (PCC). Microgrids are networked with each other through PCCs and distribution lines. With such a configuration, instead of managing massive DGUs at grid edges, a Distribution System Operator (DSO) only needs to coordinate a few PE interfaces

of microgrids [1], by which the system management complexity at the DSO level is significantly reduced. Reference [3] reports a real-world demonstration of networked microgrids.

Given the microgrid-based distribution system, an essential function of its Distribution Management System (DMS) is to assess security of networked microgrids. Specifically, such a function is expected to include the static security assessment (SSA) and transient stability assessment (TSA). The SSA scrutinizes if physical variables of networked microgrids in the quasi-steady-state time scale are within normal ranges. It is typically considered as optimization constraints when researchers develop coordination strategies of networked microgrids [4] for grid resilience enhancement and economical efficiency maximization. The TSA examines the dynamic behaviors of networked microgrids in a faster time scale. The TSA tool aims to characterize (large) disturbances that the networked microgrids can tolerate. Such characterization allows for efficient design and planning of the microgrid-based distribution systems [5], and it also enables a DSO to maintain situational awareness in real-time operation [5]. This paper focuses on assessing transient stability of *networked* microgrids. Such a topic concerns the DSO, because excessive energy transactions among microgrids may lead to stability issues, even though each individual microgrid is stabilized by its local MGCC [1].

There are several approaches to the design of TSA tools for networked microgrids. One may tailor the TSA development in bulk transmission systems for microgrid application. A prevailing TSA method in transmission systems is based on time-domain simulation [6]. In such a method, the system responses are simulated given all credible contingencies [6]. System security is evaluated by examining the responses obtained. This method can be tailored to screen out critical contingencies in networked microgrids. However, it cannot certify stability rigorously, as by definition, stability [7] requires one to examine system responses under infinite number of disturbances, which is impossible for time-domain simulation. Another TSA method developed for the transmission grid is the energy function method [8]–[10]. By assuming transmission lines are lossless, this method aims to construct an energy function that can certify stability. While the lossless-line assumption is plausible in transmission systems, it does not hold in networked microgrids due to large R/X ratios of distribution lines [1], thereby resulting in non-existence of the energy function in networked microgrids [8]. Reference [8] constructs a quadratic Lyapunov function which can be used for TSA of a power system with line loss. However, the DSO tool developed based on [8] may be overly conservative. Besides the TSA

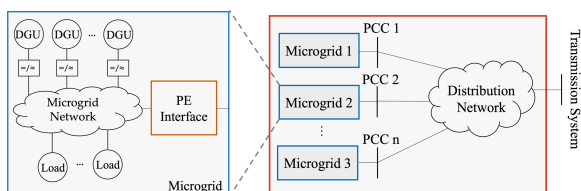


Fig. 1. A microgrid-based distribution system: inside the left blue box shows the physical structure of a microgrid.

tools developed for transmission systems, References [1], [2] develop stability assessment tools specifically for networked microgrids. Reference [2] has proposed a framework capable of assessing the small-signal stability of networked microgrids in a distributed manner, but it cannot certify the stability when large disturbances occur. Reference [1] utilizes linear matrix inequalities (LMIs) in order to certify global asymptotic stability of networked microgrids. The framework proposed in [1] requires a special form of interface dynamics and it cannot characterize disturbances that can be tolerated by networked microgrids when global asymptotic stability is not guaranteed.

In this paper, we develop a TSA tool for networked microgrids using machine learning-based Neural Lyapunov Methods. Assessing transient stability is formulated as a problem of estimating the security region of networked microgrids. We leverage neural networks to learn a local Lyapunov function in the state space. The optimal security region is estimated based on the Lyapunov function learned, and is used for characterizing disturbances that the networked microgrids can tolerate. The proposed TSA tool has the following merits: 1) It can provide less conservative characterization of disturbances that can be tolerated by networked microgrids, compared with methods based on quadratic Lyapunov functions; and 2) It can assess the transient stability of networked microgrids with heterogeneous interface dynamics.

The rest of this paper is organized as follows: Section II describes the dynamics of networked microgrids; Section III presents the neural Lyapunov method to TSA; and Section IV tests and validates the tool in three numerical experiments; and Section V concludes the paper and points out future direction.

II. DYNAMICS OF MICROGRIDS WITH PE INTERFACES

With the physical configuration of the networked microgrids in Figure 1, the dynamics that a microgrid exhibits at the DSO-level control are mainly determined by the control strategy deployed at its power electronics interface [1], [2]. One promising control strategy for the PE interface is the droop method [1]. Such a method does not need explicit communication between microgrid interfaces in order to achieve load sharing, allowing for distributed implementation [1], [11]–[13]. For the droop method deployed at a microgrid interface, some local signals are leveraged as the power balance indicators [1], and the interface response is tuned according to the measurements of these signals. Common selections of these local signals include frequency, voltage magnitude and voltage angle that are measured at the microgrid PCC. Specifically, the *frequency droop control* takes the frequency as the balance indicator for real power [12], while the *angle droop control* considers the voltage phase angle as the balance indicator [1], [11], [13].

For the n networked microgrids in Figure 1, without loss of generality, suppose that the angle droop control is deployed in the k -th microgrid's PE interface, where $k = 1, 2, \dots, n$. The interface dynamics of the k -th microgrid are [1], [2]

$$M_{ak}\dot{\delta}'_k + \delta'_k = D_{ak}(P_k^* - P_k) \quad (1a)$$

$$M_{vk}\dot{E}'_k + E'_k = D_{vk}(Q_k^* - Q_k) \quad (1b)$$

where δ'_k and E'_k are *deviations* of voltage phase angle δ_k and voltage magnitude E_k from their steady state values δ_k^*

and E_k^* at the k -th PCC, respectively, i.e., $\delta'_k := \delta_k - \delta_k^*$ and $E'_k := E_k - E_k^*$; M_{ak} and M_{vk} are tracking time constants; D_{ak} and D_{vk} are droop gains; P_k and Q_k denote real and reactive power injections to PCC k ; and P_k^* and Q_k^* are the steady-state injections of real and reactive power at the k -th PCC [1]. The n microgrids are networked via distribution network which introduces constrains

$$P_k - G_{kk}E_k^2 - \sum_{i \neq k} E_k E_i Y_{ki} \cos(\delta_{ki} - \sigma_{ki}) = 0 \quad (2a)$$

$$Q_k + B_{kk}E_k^2 - \sum_{i \neq k} E_k E_i Y_{ki} \sin(\delta_{ki} - \sigma_{ki}) = 0, \forall k, \quad (2b)$$

where $\delta_{ki} = \delta_k - \delta_i$; $G_{kk} + jB_{kk}$ is the k -th diagonal entry in the admittance matrix of the distribution network; and $Y_{ki} \angle \sigma_{ki}$ is the (k, i) -th entry of the admittance matrix. The steady-state values δ_k^* , E_k^* , P_k^* and Q_k^* are designed based on economic dispatch and they satisfy the following equality constrains:

$$P_k^* - G_{kk}E_k^{*2} - \sum_{i \neq k} E_k^* E_i^* Y_{ki} \cos(\delta_{ki}^* - \sigma_{ki}) = 0 \quad (3a)$$

$$Q_k^* + B_{kk}E_k^{*2} - \sum_{i \neq k} E_k^* E_i^* Y_{ki} \sin(\delta_{ki}^* - \sigma_{ki}) = 0, \forall k, \quad (3b)$$

where $\delta_{ki}^* = \delta_k^* - \delta_i^*$. Differential equations (1) with algebraic equations (2) characterize the dynamics of the n networked microgrids, and their compact form is

$$\dot{\mathbf{x}} = \mathbf{f}(\mathbf{x}) \quad (4)$$

where $\mathbf{x} = [\delta'_1, \delta'_2, \dots, \delta'_n, E'_1, E'_2, \dots, E'_n]$; and $\mathbf{f}(\cdot)$ is determined by (1) and (2). Note that the equilibrium point \mathbf{o} of the dynamic system (4) is the origin of the state space.

If $M_{vk} \gg M_{ak}$, the *time-scale separation* can be assumed [1], [5]. In such a case, the voltage deviation E'_k evolves much slower than the phase angle deviation δ'_k and, therefore, E'_k is assumed to be constant [1]. Furthermore, if only angular stability is of interest, the dynamics of the n networked microgrids can be described by

$$M_{ak}\dot{\delta}'_k + \delta'_k = D_{ak}(P_k^* - P_k), \forall k, \quad (5)$$

where $P_k = G_{kk}E_k^{*2} + \sum_{i \neq k} E_k^* E_i^* Y_{ki} \cos(\delta_{ki}^* + \delta_{ki}^* - \sigma_{ki})$. The compact form of (5) can be also expressed as (4) where \mathbf{x} and $\mathbf{f}(\cdot)$ should be revised accordingly. Besides, with the time-scale separation assumption, if the frequency droop control is deployed in the j -th microgrid, the j -th differential equation in (5) is replaced by

$$\dot{\delta}'_j = \omega'_j, \quad M_{fj}\dot{\omega}'_j + D_{fj}\omega'_j = P_j^* - P_j$$

where ω'_j denotes the frequency deviation from its nominal value at the j -th PCC; M_{fj} and D_{fj} are the emulated inertia and damping coefficients, respectively; and $P_j = G_{jj}E_j^{*2} + \sum_{i \neq j} E_j^* E_i^* Y_{ji} \cos(\delta_{ji}^* + \delta_{ji}^* - \sigma_{ji})$.

With the networked microgrids (4) and its equilibrium point \mathbf{o} , a DSO may have the following two questions [5]: 1) Is \mathbf{o} asymptotically stable? 2) How ‘‘large’’ are the disturbances that the networked microgrids can tolerate? The transient stability assessment framework proposed in this paper aims to answer these two questions.

III. NEURAL LYAPUNOV METHODS

This section answers the two DSO's questions. We first point out the asymptotic stability of networked microgrids can be certified by the Lyapunov linearization method [7] and formulate the second DSO's question as the one of estimating a security region of networked microgrids. Then an optimal security region is estimated via learning a Lyapunov function. Finally, how to empirically tune the parameters of proposed algorithms is discussed.

A. Asymptotic Stability Check and Security Region

Given the networked microgrids (4) and its equilibrium \mathbf{o} , the Lyapunov linearization method [7] suggests the asymptotic stability of \mathbf{o} can be determined by examining the linearized version of (4), i.e.,

$$\dot{\mathbf{x}} = A\mathbf{x}. \quad (6)$$

In (6), $A \in \mathbb{R}^{m \times m}$ is a system matrix, where m is the length of the state vector \mathbf{x} . The system matrix A is obtained by linearizing (4) around its equilibrium point \mathbf{o} based on the linearization technique. Suppose that matrix A has m eigenvalues $\lambda_1, \lambda_2, \dots, \lambda_m$. The equilibrium point \mathbf{o} of (4) is asymptotically stable [7], if

$$\text{Re}(\lambda_i) < 0 \quad \forall i = 1, 2, \dots, m. \quad (7)$$

Condition (7) answers the first question raised in Section II.

For the second DSO's question, a *security region* can be leveraged to characterize the disturbances that the networked microgrids (4) operating at \mathbf{o} are able to tolerate. The definition of a security region is as follows [5]:

Definition 1. $\mathcal{S} \subseteq \mathbb{R}^m$ is a security region if

$$\mathbf{x}(0) \in \mathcal{S} \implies \mathbf{x}(\infty) = \mathbf{0}_m \wedge \forall t(t > 0) \implies \mathbf{x}(t) \in \mathcal{S}.$$

In Definition 1, $\mathbf{x}(0)$ is resulting from the microgrid interconnection-level events, say, topology changes of distribution system network, and one of the microgrids enters an islanded/grid-connected mode; and $\mathbf{0}_m$ denotes the origin of the state space with m states. Definition 1 essentially says that the system trajectory starting in the security region \mathcal{S} will stay in \mathcal{S} and tends to the equilibrium point \mathbf{o} . The second DSO's question can be answered if such a security region is obtained.

A security region \mathcal{S} can be estimated based on a system behavior-summary function, i.e., a Lyapunov function, in conjunction with the Local Invariant Set Theorem [7]. The Lyapunov function is given by the following definition [5]:

Definition 2. A continuous differentiable scalar function $V(\mathbf{x})$ is a Lyapunov function, if, in a region $\mathcal{B}_u := \{\mathbf{x} \in \mathbb{R}^m | u > 0, \|\mathbf{x}\|_2^2 < u^2\}$, 1) V is positive definite in \mathcal{B}_u , and 2) \dot{V} is negative definite in \mathcal{B}_u .

Once a legitimate Lyapunov function $V(\mathbf{x})$ is available, a region \mathcal{S}_d can be found by

$$\mathcal{S}_d = \{\mathbf{x} \in \mathcal{B}_u | d > 0, V(\mathbf{x}) < d\}. \quad (8)$$

The region \mathcal{S}_d is an invariant set due to the decreasing nature of the Lyapunov function $V(\mathbf{x})$. Besides, the Invariant Set

Theorem [7] suggests that with the Lyapunov function $V(\mathbf{x})$, a system trajectory $\mathbf{x}(t)$ starting in \mathcal{S}_d converges to the origin of the state space. Therefore, the region \mathcal{S}_d is a security region. In order to characterize the disturbances that the networked microgrids can tolerate, the remaining questions are: 1) How to find a legitimate Lyapunov function in a valid region \mathcal{B}_u ; and 2) with a Lyapunov function valid in \mathcal{B}_u , how to make the security region \mathcal{S}_d as large as possible by tuning d in (8). These two questions are addressed in Sections III-B and III-C.

B. Learning Lyapunov Function from State Space

1) Lyapunov Function with Neural-network Structure:

We assume that a Lyapunov function candidate is a neural network. The neural network has a hidden layer and an output layer. The input of the hidden layer is the state vector $\mathbf{x} \in \mathbb{R}^m$ and the output is a vector $\mathbf{v}_1 \in \mathbb{R}^p$ where p is the number of neurons in the hidden layer. Function $g_1 : \mathbb{R}^m \rightarrow \mathbb{R}^p$ describes the relationship between \mathbf{x} and \mathbf{v}_1 and its definition is

$$\mathbf{v}_1 = g_1(\mathbf{x}) := \tanh(W_1\mathbf{x} + \mathbf{b}_1) \quad (9)$$

where $W_1 \in \mathbb{R}^{p \times m}$; $\mathbf{b}_1 \in \mathbb{R}^p$; and $\tanh(\cdot)$ is an entry-wised hyperbolic function [5]. Furthermore, we define an intermediate vector $\mathbf{c}_1 = [c_{1,1}, c_{1,2}, \dots, c_{1,p}]^T$ for the hidden layer by $\mathbf{c}_1 = W_1\mathbf{x} + \mathbf{b}_1$. For the output layer, its input is vector \mathbf{v}_1 and its output is $V_\theta \in \mathbb{R}$ which is interpreted as the Lyapunov candidate evaluated at vector \mathbf{x} . V_θ is related with \mathbf{v}_1 via function $g_2 : \mathbb{R}^p \rightarrow \mathbb{R}$ defined by

$$V_\theta = g_2(\mathbf{v}_1) := \tanh(W_2\mathbf{v}_1 + b_2) \quad (10)$$

where $W_2 \in \mathbb{R}^{1 \times p}$; and $b_2 \in \mathbb{R}$. The intermediate variable c_2 associated with the output layer is defined by $c_2 = W_2\mathbf{v}_1 + b_2$. In sum, the Lyapunov function candidate is

$$V_\theta(\mathbf{x}) = g_2(g_1(\mathbf{x})). \quad (11)$$

Denote by θ the vector that consists of all unknown entries in W_1 , \mathbf{b}_1 , W_2 , and b_2 . The subscript of V_θ indicates that the Lyapunov function candidate depends on θ .

2) *Lyapunov Risk Minimization:* We proceed to tune θ such that $V_\theta(\mathbf{x})$ in (11) meets the two conditions in Definition 2. Suppose that there are q state vectors $\mathbf{x}_1, \mathbf{x}_2, \dots, \mathbf{x}_q$. Let set \mathcal{X} collect these q vector samples. To tune θ , we introduce a cost function called (empirical) Lyapunov risk, i.e.,

$$R_q(\theta) = \frac{\alpha}{q} \sum_{i=1}^q (\text{ReLU}(-V_\theta(\mathbf{x}_i))) + \frac{\beta}{q} \sum_{i=1}^q \left(\text{ReLU}(\dot{V}_\theta(\mathbf{x}_i) + \tau) \right) + \gamma V_\theta^2(\mathbf{0}_m) \quad (12)$$

where the tunable parameters α , β , γ and τ are positive scalars; $\text{ReLU}(\cdot)$ denotes the rectified linear unit; and \dot{V}_θ is given by [5]

$$\dot{V}_\theta = \frac{\partial V_\theta}{\partial \mathbf{x}} \mathbf{f}(\mathbf{x}) = \frac{\partial V_\theta}{\partial c_2} \frac{\partial c_2}{\partial \mathbf{v}_1} \frac{\partial \mathbf{v}_1}{\partial \mathbf{x}} \mathbf{f}(\mathbf{x}). \quad (13)$$

In (13), the dynamics $\mathbf{f}(\mathbf{x})$ is provided in (4);

$$\begin{aligned} \frac{\partial V_{\theta}}{\partial c_2} &= 1 - V_{\theta}^2; \quad \frac{\partial c_2}{\partial \mathbf{v}_1} = W_2; \quad \frac{\partial c_1}{\partial \mathbf{x}} = W_1; \text{ and} \\ \frac{\partial \mathbf{v}_1}{\partial c_1} &= \text{diag}(1 - \tanh^2(c_{1,1}), \dots, 1 - \tanh^2(c_{1,p})). \end{aligned}$$

The interpretation of the Lyapunov risk (12) is presented as follows. In (12), The first ‘‘ReLU’’ term incurs positive penalty if $V_{\theta}(\mathbf{x}_i)$ is negative. The second ‘‘ReLU’’ term results to positive penalty if $\dot{V}_{\theta}(\mathbf{x}_i)$ is greater than $-\tau$. If the evaluation of V_{θ} at the origin of the state space is not zero, the Lyapunov risk also increases according to (12). Parameters α , β , γ and τ determine the importance of the three terms of (12) and their tuning procedure is discussed in Section III-D.

Given the training set \mathcal{X} , in order to find a Lyapunov function valid in \mathcal{B}_u , unknown parameters θ should be chosen such that the Lyapunov risk $R_q(\theta)$ is minimized, viz.

$$\min_{\theta} R_q(\theta). \quad (15)$$

The gradient decent algorithm can be leveraged to solve (15). Algorithm 1 presents a procedure to update θ , where θ_0 is the initial guess of θ ; $r \in \mathbb{Z}_+$ denotes the times of updating θ ; and the positive scalar η is the learning rate. Note that merely using Algorithm 1 to update θ is not sufficient even with a large r . One reason is that \mathcal{X} solely covers a finite number of training samples in \mathcal{B}_u . With the θ obtained by Algorithm 1 based on \mathcal{X} , it is possible that one or both of the two conditions in Definition 2 are violated in some part of \mathcal{B}_u that is not included in \mathcal{X} . This issue is addressed in Section III-B3.

Algorithm 1 Lyapunov Risk Minimization

```

1: function MinRisk( $\theta_0, \mathcal{X}, \mathbf{f}, p, r, \eta, \alpha, \beta, \gamma, \tau$ )
2:    $\theta \leftarrow \theta_0$ 
3:   while  $i \leq r$  do
4:     Update  $V_{\theta}$  and  $\dot{V}_{\theta}$  by (11), (13) with  $\theta$ 
5:     Compute  $R_{|\mathcal{X}|, \rho}(\theta)$  via (12) over  $\mathcal{X}$ 
6:      $\theta \leftarrow \theta - \eta \nabla_{\theta} R_{|\mathcal{X}|, \rho}(\theta)$ ;  $i \leftarrow i + 1$ 
7:   end while
8:   return  $\theta$ 
9: end function

```

3) *Augment of Training Samples*: Here, we utilize the satisfiability modulo theories (SMT) solver [14] to analytically check if the function learned by MinRisk is a legitimate Lyapunov function. This is equivalent to searching for state vectors $\mathbf{x} \in \mathcal{B}_u$ that satisfy

$$(V_{\theta}(\mathbf{x}) \leq 0 \vee \dot{V}_{\theta} \geq 0) \wedge (\|\mathbf{x}\|_2^2 \geq l^2) \quad (16)$$

where l is a small scalar; and $\|\mathbf{x}\|_2^2 \geq l^2$ is added for avoiding numerical issues of the SMT solver [15]. The state vectors $\mathbf{x} \in \mathcal{B}_u$ satisfy condition (16) are termed *counterexamples* which can be found by the SMT solver, such as dReal [14]. Denote by \mathcal{C} the set that consists of the counterexamples found by the SMT solver. If \mathcal{C} is not an empty set, the learned function is not a Lyapunov function and the richness of the training set \mathcal{X} is enhanced by adding counterexamples in \mathcal{C} to \mathcal{X} . The

procedure of augmenting the training samples is presented in the ‘‘AddSample’’ function of Algorithm 2.

The function LearnFunc of Algorithm 2 summarizes the overall procedure of updating the unknown parameter θ and augmenting the training set \mathcal{X} . In LearnFunc, n_i is the maximum iteration times defined by users.

Algorithm 2 Learning Lyapunov Function

```

1: function AddSample( $\mathcal{X}, V_{\theta}, \mathbf{f}, u$ )
2:    $\kappa \leftarrow 1$ 
3:   Check (16) in  $\mathcal{B}_u$  and find  $\mathcal{C}$  by dReal
4:   if  $\mathcal{C} = \emptyset$  then  $\kappa \leftarrow 0$     $\triangleright$  No counterexamples found
5:   else  $\mathcal{X} \leftarrow \mathcal{C} \cup \mathcal{X}$       $\triangleright$  Add counterexamples to  $\mathcal{X}$ 
6:   end if
7:   return  $\mathcal{X}, \kappa$ 
8: end function
9: function LearnFunc( $\mathcal{X}, \theta_0, \mathbf{f}, u, p, r, \eta, \alpha, \beta, \gamma, \tau, n_i$ )
10:   $\kappa \leftarrow 1$ ;  $j \leftarrow 0$ 
11:  while  $(\kappa = 1) \wedge (j \leq n_i)$  do
12:     $\theta \leftarrow \text{MinRisk}(\theta_0, \mathcal{X}, \mathbf{f}, p, r, \eta, \alpha, \beta, \gamma, \tau)$ 
13:     $\theta_0 \leftarrow \theta$ ;  $j \leftarrow j + r$ 
14:     $\mathcal{X}, \kappa \leftarrow \text{AddSample}(\mathcal{X}, V_{\theta}, \mathbf{f}, u)$ 
15:  end while
16:  if  $\kappa = 0$  then  $V_{\theta^*} \leftarrow V_{\theta} - V_{\theta}(\mathbf{0}_m)$ 
17:  else  $V_{\theta^*} \leftarrow \emptyset$ 
18:  end if
19:  return  $V_{\theta^*}$ 
20: end function

```

C. Security Region Estimation Algorithm

Given a Lyapunov function V_{θ^*} with its valid region \mathcal{B}_u , we proceed to tune d in (8) so that the estimated security region is maximized. The optimal d^* is determined by solving [10]

$$d^* = \min_{\mathbf{x}} V_{\theta^*}(\mathbf{x}) \quad (17a)$$

$$\text{s.t. } \|\mathbf{x}\|_2^2 = u^2. \quad (17b)$$

The state vectors satisfying the equality constrain (17b) constitute the boundary of the valid region \mathcal{B}_u of V_{θ^*} . Equation (17a) essentially says that d^* is the minimal value of $V_{\theta^*}(\mathbf{x})$ evaluated along \mathcal{B}_u 's boundary.

The optimization (23) can be solved by finding *critical points* defined as follows. The Lagrangian $L(\mathbf{x}, \phi)$ of (23) is

$$L(\mathbf{x}, \phi) = \phi(\|\mathbf{x}\|_2^2 - u^2) + V_{\theta^*}(\mathbf{x}). \quad (18)$$

where $\phi \in \mathbb{R}$. Define a set \mathcal{P} by

$$\mathcal{P} := \left\{ \mathbf{x} \in \mathbb{R}^m \left| \frac{\partial L(\mathbf{x}, \phi)}{\partial \mathbf{x}} = 0, \|\mathbf{x}\|_2^2 - u^2 = 0 \right. \right\}. \quad (19)$$

Each element of the set \mathcal{P} is a critical point. The global minimum of V_{θ^*} over \mathcal{B}_u 's boundary occurs at one of the critical points. Finding \mathcal{P} is equivalent to obtaining all solutions to

$$2\phi\mathbf{x} + \frac{\partial V_{\theta^*}}{\partial \mathbf{x}} = \mathbf{0}_m; \quad \|\mathbf{x}\|_2^2 - u^2 = 0. \quad (20)$$

Unknown parameters W_1 , W_2 , \mathbf{b}_1 , and \mathbf{b}_2 in (9) and (10) can be updated by the θ^* returned by Algorithm 2. Denote by W_1^* ,

W_2^* , \mathbf{b}_1^* , and \mathbf{b}_2^* the updated version of W_1 , W_2 , \mathbf{b}_1 , and \mathbf{b}_2 , respectively. In (20),

$$\frac{\partial V_{\theta^*}}{\partial \mathbf{x}} = (1 - V_{\theta^*}(\mathbf{x})^2) W_2^* W_1^* \Lambda \quad (21)$$

where $\Lambda = \text{diag}(1 - \tanh^2(c_{1,1}^*), \dots, 1 - \tanh^2(c_{1,p}^*))$, whence $[c_{1,1}^*, \dots, c_{1,p}^*]^\top = W_1^* \mathbf{x} + \mathbf{b}_1^*$. With (21), (20) becomes algebraic equations whose compact form is

$$\mathbf{h}(\mathbf{x}, \phi) = \mathbf{0}_{m+1}. \quad (22)$$

The Newton-Krylov (NK) method [16] can solve (22) for \mathbf{x} and ϕ with the initial guesses \mathbf{x}_0 and ϕ_0 on solutions. If set \mathcal{P} is available,

$$d^* = \min_{\mathbf{x} \in \mathcal{P}} V_{\theta^*}(\mathbf{x}). \quad (23)$$

Then, the corresponding security region is

$$\mathcal{S}_{d^*} = \{\mathbf{x} \in \mathcal{B}_u | V_{\theta^*}(\mathbf{x}) < d^*\}. \quad (24)$$

With the Lyapunov function learned by LearnFunc, the procedure to estimating a security region is provided by the SREst function of Algorithm 3, where $\text{NK}(\mathbf{h}, \mathbf{x}_0, \phi_0)$ denotes the procedure of solving $\mathbf{h}(\mathbf{x}, \phi) = \mathbf{0}_{m+1}$ with the initial guesses \mathbf{x}_0 and ϕ_0 using the NK method; and the NK procedure returns \mathbf{x}^* and ϕ^* which constitute a solution to $\mathbf{h}(\mathbf{x}, \phi) = \mathbf{0}_{m+1}$. The solution found by the NK procedure depends on the initial guesses \mathbf{x}_0 and ϕ_0 . To find all critical points, the SREst function repetitively solves (22) for n_{sr} times. For each time of solving (22), \mathbf{x}_0 and ϕ_0 are randomly realized. The Main function of Algorithm (3) summarizes the procedure described in Sections III-A, III-B, and III-C. Note that checking asymptotic stability of the given equilibrium (Lines 14-16 of Algorithm 3) is a prerequisite for learning a Lyapunov function and estimating an optimal security region.

D. Parameter Tuning

In Algorithm 3, the empirical settings of θ_0 , p , q , r , η , n_{sr} , n_i and τ are provided as follows: the random initial guess θ_0 is obtained by the initialization procedure reported in [17]; $p \geq 2m$; q , n_{sr} , and n_i are 500, 100, and 5000, respectively; integer $r \in [10, 30]$; $\tau \in [0.1, 0.5]$; and $\eta \in [0.01, 0.02]$.

Given a set of user-defined parameters, it is possible that the Main function returns an empty set \emptyset , meaning that the function fails to find a Lyapunov function valid in \mathcal{B}_u within n_i iterations. Solutions to such a situation include 1) decreasing

Algorithm 3 Security Region Estimation

```

1: function SREst( $V_{\theta^*}, u, n_{\text{sr}}$ )
2:    $\mathcal{P} \leftarrow \emptyset$ ; construct  $\mathbf{h}$  by (20), (21)
3:   for  $k = 1, 2, \dots, n_{\text{sr}}$  do
4:     Pick a random  $\mathbf{x}_0$  in  $\{\mathbf{x}_0 \in \mathbb{R}^m | \|\mathbf{x}_0\|_2^2 = u^2\}$ 
5:     Pick a random  $\phi_0 \in \mathbb{R}$ 
6:      $\mathbf{x}^*, \phi^* \leftarrow \text{NK}(\mathbf{h}, \mathbf{x}_0, \phi_0)$ 
7:     if  $\mathbf{x}^* \notin \mathcal{P}$  then  $\mathcal{P} \leftarrow \mathcal{P} \cup \mathbf{x}^*$ 
8:     end if
9:   end for
10:  Obtain  $\mathcal{S}_{d^*}$  via (23), (24)
11:  return  $\mathcal{S}_{d^*}$ 
12: end function
13: function Main( $\mathbf{f}, u, p, q, \theta_0, r, \eta, \alpha, \beta, \gamma, \tau, n_{\text{sr}}, n_i$ )
14:  Linearize  $\mathbf{f}$  to obtain  $A$  in (6)
15:  Compute eigenvalues  $\lambda_i$  of  $A \forall i = 1, 2, \dots, m$ 
16:  if (7) holds then ▷ Asymptotic stability check
17:    Construct  $\mathcal{X}$  by randomly picking  $q$  vectors in  $\mathcal{B}_u$ 
18:     $V_{\theta^*} \leftarrow \text{LearnFunc}(\mathcal{X}, \theta_0, \mathbf{f}, u, p, r, \eta, \alpha, \beta, \gamma, \tau, n_i)$ 
19:    if  $V_{\theta^*} \neq \emptyset$  then
20:       $\mathcal{S}_{d^*} \leftarrow \text{SREst}(V_{\theta^*}, u, n_{\text{sr}})$ 
21:      return  $V_{\theta^*}, \mathcal{S}_{d^*}$ 
22:    else Request for tuning user-defined parameters
23:    end if
24:  else Request for tuning parameters in (4)
25:  end if
26: end function

```

u ; 2) changing θ_0 ; and 3) tuning α , β , and γ . Solution 1 works because there may not be a Lyapunov function in a large ball. Solving (15) using gradient-based methods depends on the initial guess on the solution, which justifies Solution 2.

Next we present an empirical procedure to tune α , β , and γ . Denote by θ_{n_i} the n_i -th update of θ in LearnFunc. The function $V_{\theta_{n_i}}$ and its time derivative $\dot{V}_{\theta_{n_i}}$ can be visualized in subspace of \mathcal{B}_u . The visualization may suggest which condition(s) in Definition 2 is (are) violated, thereby pointing out the “direction” of tuning α , β , and γ . For example, suppose that one needs to learn a Lyapunov function for a system whose state variables are $[\delta'_1, \delta'_2, \delta'_3, \omega'_3]$ using LearnFunc. After n_i -time parameter updates, the function with parameter θ_{n_i} and its time derivative can be visualized by numerically evaluating the functions within \mathcal{B}_u 's projection to the δ'_1 - ω'_3 plane with $\delta'_2 = \delta'_3 = 0$. Suppose that the visualization is given in Figure 2. As shown in Figure 2, the function with parameter θ_{n_i} is not a Lyapunov function in $\mathcal{B}_{0.4}$, because its time derivative is not negative in $\mathcal{B}_{0.4}$, although the function is positive. Figure 2 indicates that with other parameters fixed, one may need to increase the penalty resulting from the violation of the second condition of Definition 2, i.e., increasing β in (12).

IV. NUMERICAL EXPERIMENTS

This section tests and validates the proposed method in a grid-connected microgrid, a three-microgrid interconnection with mixed dynamics, and the IEEE 123-node feeder.

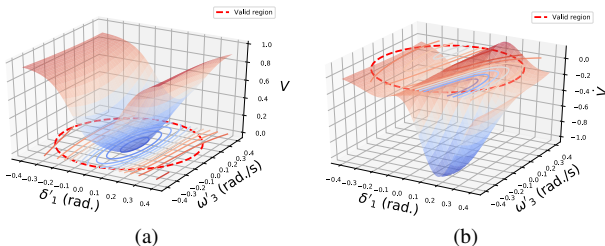


Fig. 2. Visualization of the function (a) and its time derivative (b) after n_i times of parameter update: the function is NOT a Lyapunov function.

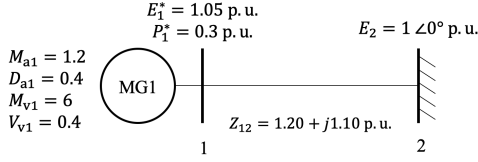


Fig. 3. A grid-connected microgrid [5]

TABLE I
USER-DEFINED PARAMETERS OF ALGORITHM 3

Case Name	p	q	n_{sr}	n_i	r	τ
A Grid-connected Microgrid	6	500	100	5000	10	0.1
Three Networked Microgrids	8	500	100	5000	30	0.1
IEEE 123-node Feeder	8	500	100	5000	10	0.5
Case Name	η	u	α	β	γ	N/A
A Grid-connected Microgrid	0.01	1.5	1	5	0	N/A
Three Networked Microgrids	0.02	0.4	3	1	3	N/A
IEEE 123-node Feeder	0.01	0.7	1	1	0	N/A

A. A Grid-connected Microgrid

Figure 3 shows a grid-connected microgrid (MG) with angle-droop control. The user-defined parameters required in Algorithm 3 are listed in Table I.

1) *Learned Lyapunov Function*: After 500 times of parameter updates, which takes 32.18 seconds, Algorithm 2 outputs a Lyapunov function. Figure 4 visualizes the Lyapunov function learned and its time derivative. As shown in Figure 4, the function learned is positive definite in the valid region $\mathcal{B}_{1.5}$ and its time derivative is negative definite in $\mathcal{B}_{1.5}$. This suggests that the function learned is a Lyapunov function in $\mathcal{B}_{1.5}$.

2) *Estimated Security Region*: Given the Lyapunov function learned with its valid region $\mathcal{B}_{1.5}$, the security region estimated by Algorithm 3 is $\mathcal{S}_{1.01}$ which is defined by (24). In Figure 5, the red-solid circle is the boundary of $\mathcal{S}_{1.01}$, while the red-dash circle is the boundary of $\mathcal{B}_{1.5}$; and the region enclosed by the red-solid circle is a security region. Besides, the SREst function suggests that d^* in (17) is 1.01 which is attained when $\delta'_1 = -0.82$ and $E'_1 = 1.26$.

We proceed to check the correctness of the estimated security region $\mathcal{S}_{1.01}$. Since the test system only has two state variables, given the Lyapunov function learned, the largest security region can be found without solving optimization (17). For example, we can visualize a security region \mathcal{S}_d with a small d , say, $d = 0.15$. Figure 5-(b) visualize $\mathcal{S}_{0.15}$. We keep increasing d gradually until the boundary of \mathcal{S}_d touches the boundary of $\mathcal{B}_{1.5}$ for the first time. As can be observed

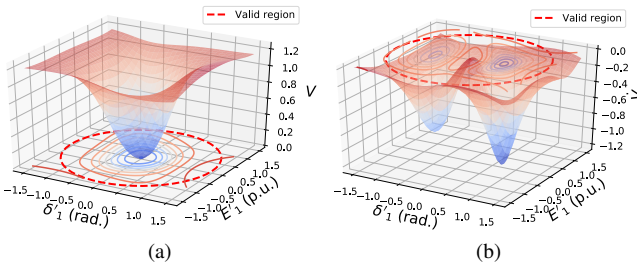
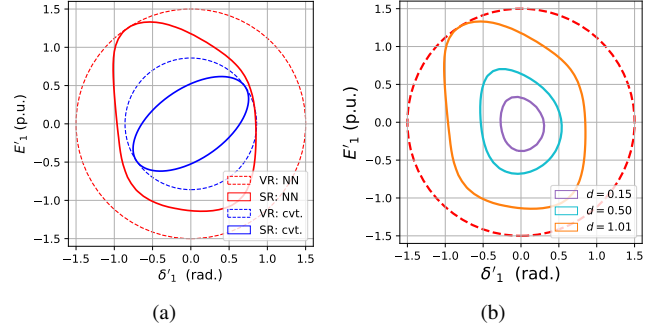


Fig. 4. (a) Lyapunov function and (b) its time derivative for a grid-tied MG

Fig. 5. (a) Comparison between the proposed (NN) and conventional (cvt.) methods: security region (SR) and valid region (VR). (b) An alternative way to find \mathcal{S}_{d^*} by tuning d .

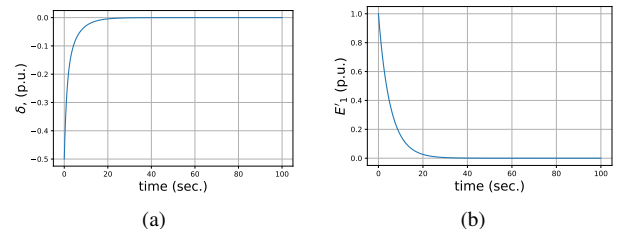
in Figure 5-(b), when $d = 1.01$, the boundaries of \mathcal{S}_d and $\mathcal{B}_{1.5}$ touch with each other at $(-0.82, 1.26)$. Therefore, $\mathcal{S}_{1.01}$ is the largest security region that can be estimated based on the learned Lyapunov function. The security region obtained by such a procedure is consistent with the one estimated by function SREst.

3) *Comparison*: The proposed method is compared with a conventional method reported in [8]. Denote by \mathcal{S}' the security region estimated based on a quadratic Lyapunov function constructed in [8]. In Figure 5, the region enclosed by the blue-solid circle is \mathcal{S}' , while the blue-dash circle is the boundary of the valid region of the quadratic Lyapunov function. It can be observed that $\mathcal{S}_{1.01}$ is larger than \mathcal{S}' . This suggests that the propose method can provide a less conservative characterization of the security region than the conventional method.

Suppose that the grid-connected MG has an initial condition $\mathbf{x}(0) = [-0.5, 1]^\top$, due to a disturbance. Such an initial condition is inside $\mathcal{S}_{1.01}$, but outside \mathcal{S}' . Therefore, $\mathcal{S}_{1.01}$ can conclude that the system trajectory tends to its equilibrium point, whereas \mathcal{S}' can conclude nothing about the system's asymptotic behavior under such a disturbance. The time-domain simulation shown in Figure 6 confirms that all state variables tend to their pre-dispatched steady-state values.

B. Three Networked Microgrids with Mixed Dynamics

Figure 7 shows a three-MG interconnection with mixed interface dynamics: the angle droop control is deployed in the PE interfaces of MGs 1 and 2, whereas the frequency droop control is deployed in the PE interfaces of MG 3.

Fig. 6. Time-domain simulation for the grid-connected MG with initial conditions $\delta'_1(0) = -0.5$ rad. and $E'_1(0) = 1$ p.u.

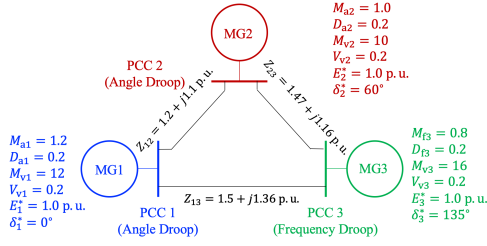


Fig. 7. Three Networked Microgrids with Mixed Dynamics

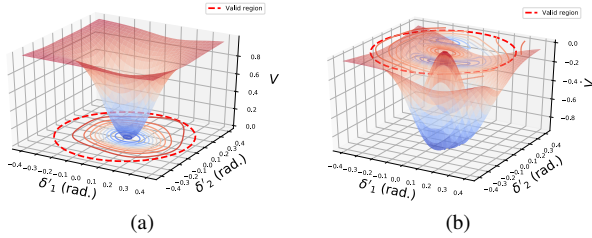


Fig. 8. (a) Lyapunov function and (b) time derivative for 3 networked MGs

Since $M_{vk} \gg M_{ak}$ for $k = 1, 2$ and $M_{v3} \gg M_{f3}$, the time-scale separation is assumed [1]. We focus on the asymptotic behavior of phase angle and frequency. The user-defined parameters of Algorithm 3 are listed in Table I.

1) *Learned Lyapunov Function*: In this experiment, after 2790 times of parameter updates, which takes 23737.53 seconds, Algorithm 3 outputs a Lyapunov function V_{θ^*} valid in $\mathcal{B}_{0.4}$. Given $\delta_3' = 0$ and $\omega_3' = 0$, V_{θ^*} and \dot{V}_{θ^*} are visualized in Figure 8 where it is observed that $V_{\theta^*} > 0$ and $\dot{V}_{\theta^*} < 0$ in $\mathcal{B}_{0.4}$, suggesting V_{θ^*} behaves like a Lyapunov function.

2) *Estimated Security Region*: With the learned Lyapunov function, Algorithm 3 provides an estimated security region $\mathcal{S}_{0.37}$. Figure 9-(a) visualizes $\mathcal{S}_{0.37}$ and $\mathcal{B}_{0.4}$ in the δ_1' - δ_2' space with $\delta_3' = 0.37$ and $\omega_3' = -0.14$, where the red-solid circle is the boundary of $\mathcal{S}_{0.37}$, and the red-dash circle is the boundary of $\mathcal{B}_{0.4}$. The SREst function suggests that d^* in (17) is 0.37 which is attained when \mathbf{x} is $[-0.07, 0.01, 0.37, -0.14]^\top$. Figure 9-(a) shows that the boundary of $\mathcal{S}_{0.37}$ touches the boundary of $\mathcal{B}_{0.4}$ at point $(-0.07, 0.01)$.

3) *Comparison*: Denote by \mathcal{S}'' the security region estimated based on the Lyapunov function proposed in [8]. The blue-solid circle in Figure 9-(b) represents the boundary of

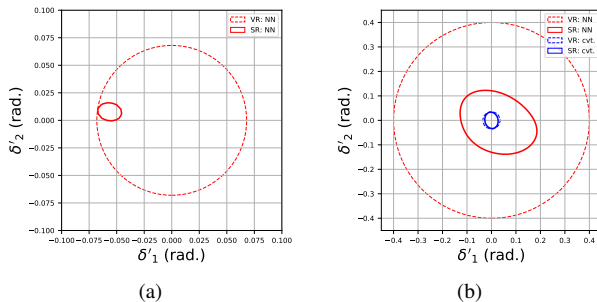


Fig. 9. (a) Security region (SR) and valid region (VR) around the touching point. (b) Comparison between the proposed (NN) and conventional (cvt.) methods.

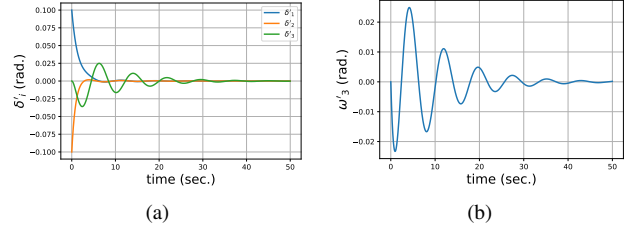


Fig. 10. Time-domain simulation of the 3 networked MGs with $\mathbf{x}(0) = [0.1, -0.1, 0, 0]^\top$: (a) angle deviation and (b) frequency deviation.

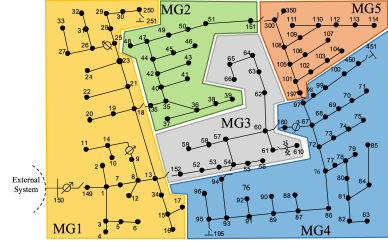


Fig. 11. IEEE 123-node Test Feeder [1]

\mathcal{S}'' in the δ_1' - δ_2' plane, given $\delta_3' = \omega_3' = 0$. Suppose that the pre-event condition $\mathbf{x}(0)$ is $[0.1, -0.1, 0, 0]^\top$. Since $\mathbf{x}(0)$ is inside $\mathcal{S}_{0.37}$ but outside \mathcal{S}'' , one can conclude that *all states tend to the equilibrium based on $\mathcal{S}_{0.37}$, while the asymptotic behavior the system cannot be assessed by \mathcal{S}'' with $\mathbf{x}(0)$* . The time-domain simulation confirms that all state variables indeed converge to their post-event steady-state values.

C. IEEE 123-node Test Feeder

Figure 11 shows a 123-node distribution system [18] which is partitioned into 5 networked MGs [1]. We assume that each MG is managed by its MGCC and connects to the grid via a PE interface with angle droop control [1]. The impedances of the interconnection distribution lines are reported in Table II. The control parameters and pre-dispatched setpoints are listed in Table III. The user-defined parameters in Algorithm 3 are reported in Table I. Note that the time-scale separation is assumed, as $M_{vk} \gg M_{ak}$ for $k = 1, 2, \dots, 5$ in Table III.

TABLE II
DISTRIBUTION LINE PARAMETERS

From-node #	To-node #	R (p.u.)	X (p.u.)
18	135	1.2030	1.1034
13	152	1.0300	0.7400
151	300	1.4512	1.3083
54	94	1.5042	1.3554
97	197	1.4680	1.1550

1) *Online Application of Estimated security region*: Suppose that at time $t = 0$, MG 5 enters an islanded mode and the DSO would like to know if the remaining 4 networked MGs can be stabilized at a pre-dispatched operating point. During offline planning, Algorithm 3 computes a Lyapunov function V_{θ^*} and a security region $\mathcal{S}_{0.69}$ for the contingency. $\mathcal{S}_{0.69}$ can be leveraged during real-time operation, in order to determine if the remaining MGs can tolerate the disturbance due to

TABLE III
CONTROL PARAMETERS, PRE-EVENT MEASUREMENTS AND POST-EVENT SETPOINTS OF THE IEEE 123-NODE FEEDER

	MG1	MG2	MG3	MG4	MG5
M_{ak}	1.2	1	0.8	1	1.2
D_{ak}	1.2	1.2	1.2	1.2	1.2
M_{vk}	12	10	16	10	12
D_{vk}	0.2	0.2	0.2	0.2	0.2
Pre-event δ_k (rad.)	0	-0.8472	2.3062	0.5936	0.7732
δ_k^* (rad.)	0	-1.0472	2.3562	0.5236	N/A
E_k^* (p.u.)	1.0	1.0	1.0	1.0	N/A

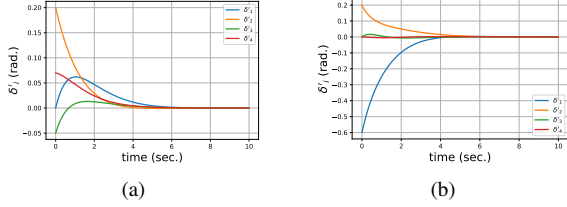


Fig. 12. Time-domain simulation of interface variables in the 123-node feeder: (a) with MG 5 islanded; (b) with $\mathbf{x}(0) = [-0.6, 0.2, 0, 0]^T$ rad.

islanding of MG 5. The initial condition $\mathbf{x}(0)$ can be obtained by collecting pre-event measurements at the MG interfaces. In this case study, $V_{\theta^*}(\mathbf{x}(0)) = 0.12 < 0.69$, suggesting that $\mathbf{x}(0) \in \mathcal{S}_{0.69}$. Thus, without any simulation, the DSO can almost instantaneously conclude that all interface variables tend to their pre-dispatched values. Such a conclusion is confirmed by the time-domain simulation in Figure 12-(a).

2) *Learned Lyapunov Function and Estimated Security Region*: It takes 2901.69 seconds to learn the Lyapunov function V_{θ^*} . Figure 13 visualizes V_{θ^*} and \dot{V}_{θ^*} . With V_{θ^*} , SREst computes a security region which is visualized in Figure 14 and it suggests that the solution to (17) is $[-0.66, 0.03, 0.06, 0.22]^T$. Figure 14-(a) visualizes the region $\mathcal{S}_{0.69}$ in the δ'_1 - δ'_2 plane with $\delta'_3 = 0.06$ and $\delta'_4 = 0.22$. It is observed that the touching point of the boundaries of $\mathcal{S}_{0.69}$ and $\mathcal{B}_{0.7}$ is $(0.66, 0.03)$.

3) *Comparison*: The comparison between the security region estimated based on the proposed and conventional methods is shown in Figure 14-(b). Denoted by \mathcal{S}''' is the security region estimated based on the conventional approach. Suppose that pre-event operating condition $\mathbf{x}(0)$ is $[-0.6, 0.2, 0, 0]^T$. Such a condition is outside \mathcal{S}''' but inside $\mathcal{S}_{0.69}$. Therefore, $\mathcal{S}_{0.69}$ can conclude that *the system trajectory will converge to the equilibrium whereas \mathcal{S}''' cannot*. The time-domain simulation shown in Figure 12-(b) confirms the convergence of the states given the pre-event condition.

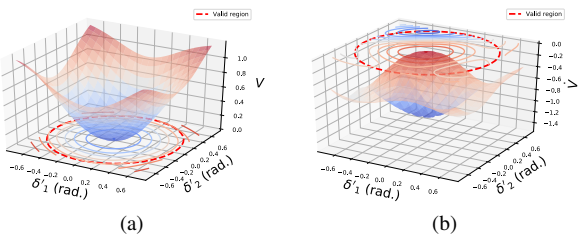


Fig. 13. (a) V_{θ^*} and (b) \dot{V}_{θ^*} in the 123-node feeder.

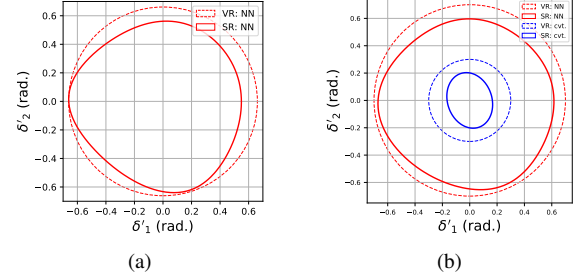


Fig. 14. (a) security region (SR) and valid region (VR) around the touching point with $\delta'_3 = 0.06$ and $\omega'_3 = 0.22$; (b) comparison between the proposed (NN) and conventional (cvt.) methods with $\delta'_3 = \omega'_4 = 0$.

V. CONCLUSION

In this paper, we propose a TSA tool for networked microgrids based on Neural Lyapunov Methods. Assessing transient stability is formulated as a problem of estimating the security region of networked microgrids. We use neural networks to learn a Lyapunov function in the state space. The optimal security region is estimated based on the function learned, and it can be used for both offline design and online operation. The effectiveness of the proposed TSA tool is tested and validated in 3 scenarios: 1) a grid-connected microgrid, 2) a three networked microgrids with heterogeneous dynamics, and 3) the IEEE 123-node test feeder. In the proposed TSA tool, the SMT solver is used to augment the training set, which is computationally expensive. Future work will develop more efficient algorithms to speed up the procedure of learning a Lyapunov function in larger systems.

REFERENCES

- [1] Y. Zhang *et al.*, "A transient stability assessment framework in power electronic-interfaced distribution systems," *TPWRS*, 2016.
- [2] —, "Interactive control of coupled microgrids for guaranteed system-wide small signal stability," *IEEE Trans. on Smart Grid*, 2016.
- [3] M. Shahidehpour *et al.*, "Networked microgrids: Exploring the possibilities of the iit-bronzeville grid," *IEEE P&E Magazine*, 2017.
- [4] M. N. Alam *et al.*, "Networked microgrids: State-of-the-art and future perspectives," *IEEE Transactions on Industrial Informatics*, 2019.
- [5] T. Huang *et al.*, "A neural lyapunov approach to transient stability assessment in interconnected microgrids," in *HICSS-54*, 2021.
- [6] K. Morison *et al.*, "Power system security assessment," 2004.
- [7] J.-J. E. Slotine, W. Li *et al.*, *Applied nonlinear control*, 1991.
- [8] H. Chiang, "Study of the existence of energy functions for power systems with losses," *IEEE Trans. on Circuits and Systems*, 1989.
- [9] H. Chiang *et al.*, "Direct stability analysis of electric power systems using energy functions: theory, applications, and perspective," 1995.
- [10] T. L. Vu *et al.*, "Lyapunov functions family approach to transient stability assessment," *TPWRS*, 2016.
- [11] R. Kolluri *et al.*, "Power sharing in angle droop controlled microgrids," *TPWRS*, 2017.
- [12] Y. Khayat *et al.*, "On the secondary control architectures of ac microgrids: An overview," *IEEE Trans. on Pow. Electro.*, 2020.
- [13] Y. Pan *et al.*, "Stability region of droop-controlled distributed generation in autonomous microgrids," *IEEE Trans. on Smart Grid*, 2019.
- [14] S. Gao *et al.*, "Delta-complete decision procedures for satisfiability over the reals."
- [15] Y.-C. Chang *et al.*, "Neural lyapunov control," in *NeurIPS 32*, 2019.
- [16] D. Knoll *et al.*, "Jacobian-free newton krylov methods: a survey of approaches and applications," *Journal of Computational Physics*, 2004.
- [17] K. He *et al.*, "Delving deep into rectifiers: Surpassing human-level performance on imagenet classification," in *ICCV*, 2015.
- [18] K. P. Schneider *et al.*, "Analytic considerations and design basis for the ieeec distribution test feeders," *TPWRS*, 2018.